

PROBING IN-MEDIUM VECTOR MESONS BY DILEPTONS AT HEAVY-ION COLLIDERS*

M. I. KRIVORUCHENKO

*Institute for Theoretical and Experimental Physics, B. Chermushkinskaya 25
117259 Moscow, Russia*

E-mail: mikhail.krivoruchenko@itep.ru

An introduction to physics of in-medium hadrons with special emphasis towards modification of vector meson properties in dense nuclear matter is given. We start from remarkable analogy between the in-medium behavior of atoms in gases and hadrons in nuclear matter. Modifications of vector meson widths and masses can be registered experimentally in heavy-ion collisions by detecting dilepton spectra from decays of nucleon resonances and light unflavored mesons including ρ - and ω -mesons. Theoretical schemes for description of the in-medium hadrons are reviewed and recent experimental results of the NA60 and HADES collaborations on the dilepton production are discussed.

Keywords: Heavy-ion collisions; vector mesons; dileptons.

1. Introduction

Elementary particles as ground-state excitations are characterized differently in the vacuum and in the dense matter. This effect is known from the solid state physics where elementary excitations are traditionally called *quasi-particles* to indicate medium-induced modifications. The medium effects manifest themselves in a wide range of physical phenomena ranging from shifts and broadening of energy levels of pionic atoms to matter-affected neutrino oscillations.

In-medium modifications of hadron properties are of special interest in order to test QCD at finite densities and temperatures and, in particular, for better understanding of the chiral and quark-hadron phase transitions and QCD confinement problem. Heavy-ion collisions provide a unique possibil-

*Lecture given at the 42-nd Predeal International Summer School in Nuclear Physics *Collective Motion and Phase Transitions in Nuclear Systems*, 28 August - 9 September, Predeal, Romania.

ity to create nuclear matter under extreme conditions and to study hadron physics around phase transitions points. One of the best direct probes to measure in-medium masses and widths of vector mesons are dileptons e^+e^- or $\mu^+\mu^-$ which, being produced, leave the reaction zone essentially undistorted by final-state interactions.

The key problem is the dependence of elementary excitations on density and temperature. The knowledge of such dependence allows to use elementary particles as probes to measure thermodynamical properties of highly compressed nuclear matter, improving thereby our knowledge of QCD, nuclear physics and the phenomenology of strong interactions.

In this lecture we discuss main effects leading to modifications of in-medium spectral functions of hadrons. In the next Sect., a remarkable analogy between atoms in gases and hadrons in nuclear matter is discussed. In Sect. 3, we show how the concept of collision broadening of particles, originated from the atomic physics, applies to behavior of nucleon resonances in nuclear matter. Sects. 4 and 5 provide a summary, respectively, of theoretical and experimental works on in-medium modifications of vector mesons and dilepton production. Sect. 6 deals with elementary sources of dileptons. The extended vector meson dominance model (eVMD) is formulated in Sect. 7 and its gauge invariance is proved in Sect. 8. Sect. 9 discusses the recent experimental results (summer 2006) from the NA60 and HADES collaborations.

2. Atoms in gases

The concept of collision broadening is discussed in atomic physics since last century. The physics behind the modifications of atomic spectral lines in gases represents the obvious theoretical interest, because it has significant features in common with physics of behavior of hadrons in nuclear matter.

2.1. Radiation damping

It is known that radiative damping results to finite widths of atomic spectral lines. The energy deposited during transition to a lower energy state can never be monochromatic, but distributed according to the Lorentz formula

$$dI(\omega) = \frac{I}{2\pi} \frac{\Gamma d\omega}{(\omega - \omega_0)^2 + (\Gamma/2)^2} \quad (1)$$

where

$$\Gamma = \Gamma_a + \Gamma_b, \quad (2)$$

with Γ_a and Γ_b being the vacuum widths of levels a and b , respectively, and $\omega_0 = E_a - E_b$ is the transition energy.

Recall its quantum-mechanical derivation: The wave function of state a equals $\Psi \sim \exp(-iE_a t - \frac{1}{2}\Gamma_a t)$, similarly for b . Transition amplitude $a \rightarrow b$ + photon of energy ω is given by $A_{ba} \sim (\exp(-i\omega t)\Psi_b)^* \Psi_a$. Evaluation of the integral $\int_{-\infty}^{+\infty} |A_{ba}|^2 dt$ gives spectral density (1).

Radiation damping is inherent to any radiating system. It results to broadening of spectral lines of isolated atoms. Thermal motion of atoms and collisions of particles affect the profile of lines also.

2.2. Doppler effect

Doppler effect results to an additional broadening of spectral lines due to motion of atoms in gases. It has a purely kinematic origin.

2.3. Collision broadening

Lorentz attributed collision broadening of spectral lines to a decoherence effect accompanied scattering of a probing atom with surrounding atoms and electrons (see e.g.,¹ Chap. 10). Consider an excited atom which experiences at random times t_i collisions with surrounding particles. Its emission intensity is summed up coherently between two collisions for $\tau \in [t_i, t_{i+1}]$ and decoherently with respect to time intervals $[t_i, t_{i+1}]$. One has

$$dI(\omega) \sim \frac{d\omega}{2\pi N} \sum_{i=1}^N \left| \int_{t_i}^{t_{i+1}} dt \exp(-i(\omega - \omega_0)t - \frac{\Gamma}{2}t) \right|^2. \quad (3)$$

One has to assume further that waiting times for sequential collisions $\tau_i = t_{i+1} - t_i$ are distributed exponentially

$$dW(\tau) = \frac{d\tau}{\tau_0} \exp(-\tau/\tau_0). \quad (4)$$

Such a hypothesis is equivalent to the requirement of the Poisson distribution of surrounding uncorrelated particles, τ_0 has the meaning of collision time. Replacing the average over collisions $\frac{1}{N} \sum_{i=1}^N \dots$ with the integral $\int dW(\tau) \dots$, one arrives at the Lorentz formula (1), with Γ replaced by $\Gamma^{total} = \Gamma + 2/\tau_0$.

According to Eq.(2), the radiation width Γ represents the sum of radiation widths of levels a and b , so one has to split $2/\tau_0$ among two levels:

$$\Gamma_a^{total} = \Gamma_a + 1/\tau_0 \quad (5)$$

4

and similarly for b . The value

$$\Gamma_{coll} = 1/\tau_0 \quad (6)$$

is called *collision width*.

We wish to bring attention to two circumstances inherent to the above approach:

- Collision broadening is physically attributed to decoherence.
- The coefficient at $1/\tau_0$ in Eq.(6).

The modern schemes use field-theoretic methods which do not refer to decoherence, although predict additional broadening inverse proportional to τ_0 in the exact agreement with the Lorentz theory. The interplay between the decoherence assumption and field-theoretic methods is interesting. The collision width is determined as an imaginary part of (obviously coherent) sum of forward scattering amplitudes with surrounding particles. Due to the quantum-mechanical optical theorem, it is equal to noncoherent sum of cross sections with surrounding particles. The coefficient at $1/\tau_0$ appears to be exact, although Eq.(6) is derived using assumptions of the *instantaneous* interactions and the *decoherence* which are not immediately evident. In the first order to the density, however, there are no corrections to Eq.(6) provided cross sections are calculated quantum-mechanically. The results of the Lorentz theory are therefore recovered using the field-theoretic methods.

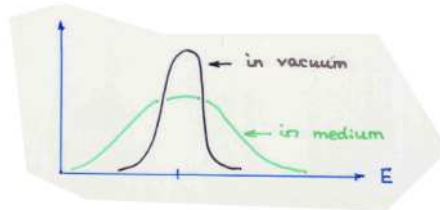


Fig. 1. Schematic representation of broadening of atomic energy levels in gases.

It is instructive to follow an elementary approach of Ref.²

The free path length ℓ_f of a hydrogen atom (or any other particle) in a gas with density n is determined by its cross section σ for scattering with other particles (atoms, molecules, ions, and electrons). There should be one particle inside of a cylinder of height ℓ_f and base σ . This condition gives

$$\ell_f = \frac{1}{n\sigma}. \quad (7)$$

The disappearance of atoms from atomic beam as a function of distance ℓ is described by an exponential law. Let a hydrogen atom in a state a moves with velocity v , then $\ell = vt$. One finds

$$N_a(\ell) = N_a(0) \exp(-\ell/\ell_f) \quad \& \quad \ell = vt \quad \Rightarrow \quad N_a(t) = N_a(0) \exp(-n\sigma vt).$$

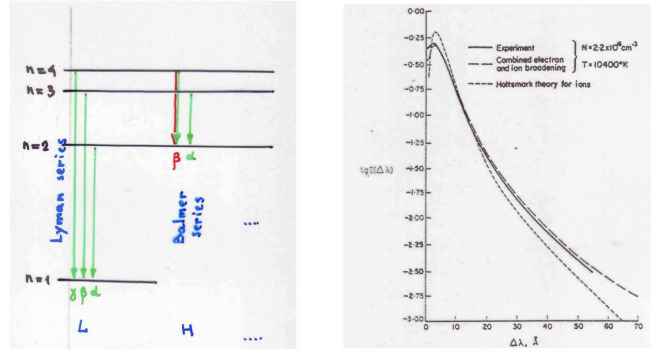


Fig. 2. **Left panel:** Schematic representation of hydrogen atom energy levels and the associated Lyman (L) and Balmer (H) series $\alpha, \beta, \gamma, \dots$ **Right panel:** Logarithm of the spectral density of the H_β line of hydrogen-like atom HeI at density of $n = 2.2 \times 10^{16} \text{ cm}^{-3}$ and temperature of $T = 10400 \text{ K}$ as a function of the wavelength shift $\Delta\lambda = \lambda - \lambda_0$ where $\lambda_0 = 1/\omega_0$. The solid line is the experiment. The dashed lines show theoretical predictions. The spectral density is broadened by a few \AA and has two peaks at $\Delta\lambda \sim \pm$ a few \AA (from Ref.³).

In quantum mechanics, decays of a quasistationary state a are governed by equation

$$|\Psi_a(t)|^2 = |\Psi_a(0)|^2 \exp(-\Gamma_a t). \quad (8)$$

This equation looks like the one describing the disappearance of particles from beam due to collisions. Since two distinct mechanisms exist for the disappearance and $N_a(t) \sim |\Psi_a(t)|^2$, the right idea is to combine two widths:

$$\Gamma_a^{total} = \Gamma_a + \Gamma_{coll} \quad (9)$$

where $\Gamma_{coll} = n\sigma v = 1/\tau_0$ is the collision width.

If resonance is placed in a medium, it acquires an additional broadening. Its spectral function modifies accordingly, as shown schematically on Fig. 1.

Collision broadening modifies spectral functions of resonances.

These ideas are in agreement with the uncertainty relation:

$$\Delta E \geq \frac{1}{\tau_0} = \frac{v}{\ell_f} = n\sigma v = \Gamma_{coll}. \quad (10)$$

Experimentally it is not possible to resolve transition energy between two atomic levels with accuracy ΔE better than the inverse collision time τ_0 . If we would ask an experimentalist to construct an experimental distribution of photon energies (wavelengths) e.g. in the Balmer β -line, he could present something resembling the curves on Fig. 1.

2.4. *Experimental observations of modified profiles of atomic spectral lines*

Shifts of energy levels and collision broadenings of atoms are observed experimentally in gases. Let us provide a couple of illustrations. Fig. 2 (left) recalls the structure of the hydrogen atom energy levels and the associated transitions and shows (right) the *modified* spectral density of the H_β line of a hydrogen-like atom in a gas.

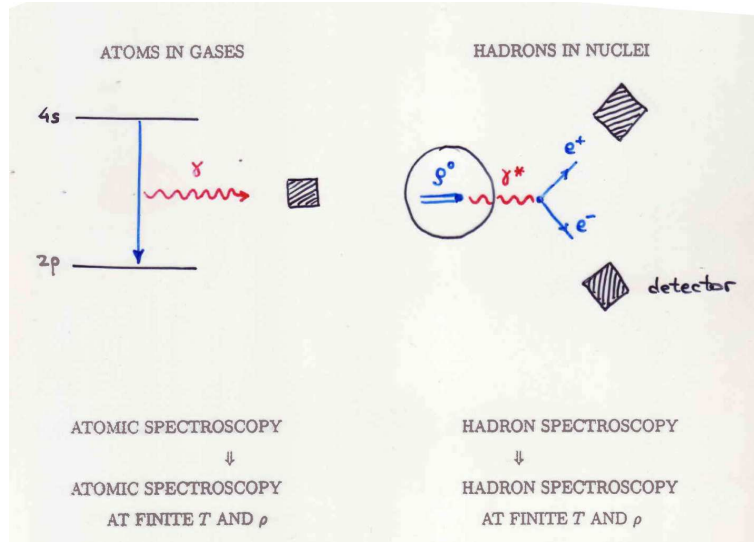


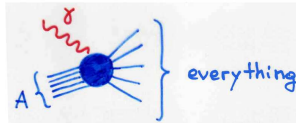
Fig. 3. Remarkable analogy between atomic spectroscopy and hadron spectroscopy.

3. Nucleon resonances in nuclei

After clarifying principal issues of spectroscopy of isolated atoms and molecules (as a result of which quantum mechanics appeared), atomic

physics evolved towards studying the in-medium modifications of atoms at finite temperature and density. Physics of intermediate energies ~ 1 GeV follows in its evolution the general trend of atomic physics with a time lag ~ 70 years. Last 15 years, new possibilities occurred to accomplish experimentally similar program for hadron spectroscopy. This analogy is illustrated in Fig. 3.

In nuclear physics, an example of broadening of resonance profiles is delivered by experiments on photoabsorption on nuclei:⁴



The photoabsorption cross sections on free nucleons ($A = 1$) develop clear peaks associated to various nucleon resonances $R = \Delta(1232), N^*(1440), \dots$ (see Fig. 4). The resonance widths are related physically to $R \rightarrow N\pi, N\pi\pi$ decays e.g. to radiation damping of Sect. 2.1.

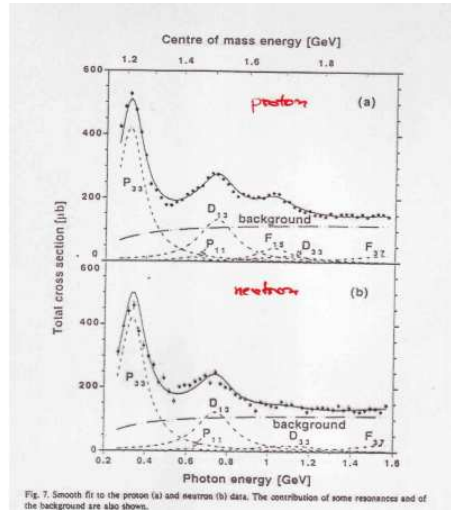


Fig. 4. Total photoabsorption cross section on proton (a) and neutron (b) vs photon energy. Contributions of various nucleon resonances and the background are shown (from Ref.²).

In nuclear environment, the Doppler effect (Sect. 2.2) related to the Fermi motion of nucleons and collision broadening (Sect. 2.3) come into play. The result is presented on Fig. 5.

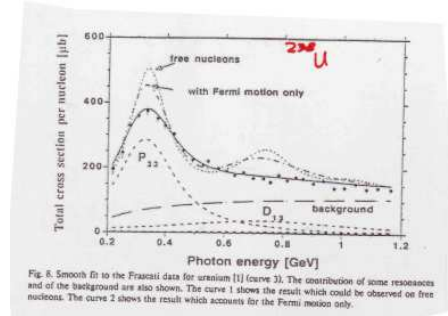


Fig. 5. Total photoabsorption cross section on ^{238}U versus photon energy in the laboratory system. Contributions of various nucleon resonances $R = \Delta(1232), N^*(1440), \dots$ and the background (long-dashed curve) are shown. The additional broadening is related to the Doppler effect (Fermi motion) and collision broadening. The Pauli blocking effect is included. The modification of the in-medium spectral density of resonances is clearly seen. Resonances heavier than $\Delta(1232)$ are broadened and masked by the background (from Ref.²).

4. In-medium properties of vector mesons: Theoretical models

The change of the nucleon mass in nuclear matter was discussed first in the pioneering works by Walecka and Chin^{5,6} already in the 1970's. The Mean Field and Relativistic Mean Field (RMF) approximations were developed to treat the dense matter self-consistently to all orders in the density. The effective nucleon mass was found to decrease significantly in nuclei at saturation density. This effect predicted by phenomenological models is confirmed by the developments of QCD.

During the last decade, the problem of the description of hadrons in dense and hot nuclear matter received new attention due to the possibility to test theoretical predictions with heavy-ion experiments. This problem is related to chiral symmetry breaking and QCD confinement. Being intrinsically non-perturbative, the number of available theoretical schemes is limited. The knowledge of the non-perturbative QCD comes in particular from lattice simulations. However, lattice results suffer still from uncertainties due to finite lattice size effects and the proper inclusion of fermions. An important role is played by field theoretical models which incorporate fundamental features of QCD.

The model proposed by Walecka⁵ was further analyzed in Refs.⁶⁻⁸ to study the in-medium vector mesons. The Nambu-Jona-Lasinio (NJL) model was introduced in the sixties as a theory of interacting nucleons⁹ and later

it was reformulated in terms of quark degrees of freedom. This model was used by the Tübingen group¹⁰ to study matter under the extreme conditions. The movement towards the chiral symmetry restoration is reliably described within the NJL model.¹¹ QCD sum rules provide a successful analytic tool to work in the non-perturbative regime. The medium modifications of hadrons are discussed in QCD sum rules at finite temperature and density.^{12–16} The vector self-energy and the effective nucleon mass at saturation density agree with those obtained by the conventional methods of nuclear physics. The values of QCD condensates and the nucleon expectation values of the various quark operators including the chiral order parameter can be determined within this approach.^{17,18}

Dispersion theory combined with the optical potential method has been used by Weise et al.^{16,19,20} to calculate mass shifts, broadening and spectral densities for vector mesons in the presence of nucleons and pions at finite density and temperature. The experimental data on the total cross sections are used to saturate the scattering amplitude at low energies with resonances. However, the obtained results are at variance with.²¹ Unitarized thermal chiral perturbation theory has been used in.^{22,23} There one matches unitarized amplitudes smoothly with the ChPT loop expansion in the low-energy region. The estimates show, in particular, mass shifts and a clear increase of the thermal widths of unflavored mesons which have relevance within the context of ultra-relativistic heavy-ion collisions. Other attractive phenomenological models for the in-medium unflavored and charmed mesons have also been proposed in.^{21,24–27}

The current status of the Brown-Rho scaling²¹ has recently been discussed by Brown and Rho.¹¹

5. In-medium properties of vector mesons: Experiments on dilepton production

The available experiments on the dilepton production are summarized in Table 1.

The dilepton spectra measured by the CERES²⁹ and HELIOS-3³⁰ Collaborations at CERN SPS found a significant enhancement of the low-energy dilepton yield below the ρ and ω peaks²⁹ in heavy systems ($Pb+Au$) as compared to light systems ($S+W$) and proton induced reactions ($p+Be$). Theoretically, this enhancement can be explained assuming a dropping mass scenario for the ρ meson and the inclusion of in-medium spectral functions for the vector mesons.^{35,36} The enhanced low energetic dilepton yield originates to most extent from an enhanced contribution of the $\pi^+\pi^-$ annihi-

Table 1. The enhanced production of dileptons in low and intermediate mass continuum. The fifth column shows intervals of invariant masses of dileptons. O/E is the ratio between integral numbers of observed and expected dileptons.

Collaboration	Ref.	E/A [GeV]	Dileptons	M [GeV]	O/E
NA38 at CERN	28	200 - 450	$\mu^+\mu^-$	0.6 - 6	~ 1.5
CERES	29	200 - 450	e^+e^-	0.05 - 1.4	5 ± 3
HELIOS-3	30	200 - 450	$\mu^+\mu^-$	0.3 - 4	~ 2.5
DLS at BEVALAC	31	1 - 5	e^+e^-	0.05 - 1	$2 - 3$
KEK	32	12	e^+e^-	0.05 - 2	~ 2
NA60	33	160	$\mu^+\mu^-$	0.2 - 1.2	~ 2
HADES at GSI	34	1 - 2	e^+e^-	0.05 - 1	~ 1

lation channel. An alternative scenario is the formation of a quark-gluon plasma in the heavy systems which leads to additional contributions to the dilepton spectrum from perturbative QCD (p QCD) such as quark-antiquark annihilation or gluon-gluon scattering.^{35,37}

The dilepton mass spectrum measured at KEK in $p + A$ reactions at the beam energy of 12 GeV³² revealed an excess of the dileptons below the ρ -meson peak over the known sources. These data were analyzed in Ref.³⁸ with no success to reproduce the experimental spectrum within a dropping mass scenario's and/or a significant collision broadening of the vector mesons.

The results of the DLS,³¹ NA60,³³ and HADES³⁴ collaborations are discussed in Sect. 9.

6. Elementary sources of dileptons

The direct decay mode $\rho, \omega \rightarrow e^+e^-$ represents a signal. There are many other sources, however, which constitute a background and which should accurately be subtracted.

6.1. Dilepton modes in decays of light unflavored mesons

One has to distinguish between vector, pseudoscalar and scalar mesons $\mathcal{M} = V, P, S$, respectively, where

$$V = \rho, \omega, \phi; \quad P = \pi, \eta, \eta'; \quad S = f_0(980), a_0(980).$$

Decay modes are presented below:

$V \rightarrow e^+e^-$		Direct decays	
$P \rightarrow \gamma e^+e^-$	$S \rightarrow \gamma e^+e^-$	Dalitz decays	
$V \rightarrow P e^+e^-$	$P \rightarrow V e^+e^-$	Dalitz decays	
$V \rightarrow P P e^+e^-$	$P \rightarrow P P e^+e^-$	$S \rightarrow P P e^+e^-$	Four-body decays

The photon and dilepton branching ratios are calculated using the effective meson theory.³⁹ Mesons are produced in NN and πN collisions. The reactions of rescattering, absorption and reabsorption of mesons affect the observed dilepton yield.

6.2. Dilepton modes in decays of nucleon resonances

Besides light unflavored mesons $\mathcal{M} = V, P, S$, nucleon resonances $R = \Delta(1232), N^*(1440), \dots$ are produced in the course of heavy-ion collisions. Their decays contribute to the measured dilepton spectra.

The $\Delta(1232)$ Dalitz decay is one of the major sources of dileptons in heavy-ion collisions at intermediate energies.^{40–42} The first correct calculation of that decay is given only recently,⁴³ while kinematically complete expressions for Dalitz decays of other positive and negative parity high-spin resonances are given in Ref.⁴⁴

In order to evaluate the Delta Dalitz decay rate, HADES³⁴ used one of six pairwise different incorrect expressions available in literature before.⁴³ We present therefore results of Ref.⁴³

The Δ resonance width for decay into nucleon and a virtual photon is given by

$$\Gamma(\Delta \rightarrow N\gamma^*) = \frac{\alpha}{16} \frac{(m_\Delta + m_N)^2}{m_\Delta^3 m_N^2} ((m_\Delta + m_N)^2 - M^2)^{1/2} ((m_\Delta - m_N)^2 - M^2)^{3/2} \left(G_M^2 + 3G_E^2 + \frac{M^2}{2m_\Delta^2} G_C^2 \right). \quad (11)$$

Here, m_N and m_Δ are nucleon and Δ masses, $M^2 = q^2$ is the photon four-momentum, G_M , G_E , and G_C are magnetic, electric and Coulomb transition form factors.

The factorization prescription allows to find the dilepton decay rate of the Δ resonance:

$$d\Gamma(\Delta \rightarrow N e^+ e^-) = \Gamma(\Delta \rightarrow N\gamma^*) M \Gamma(\gamma^* \rightarrow e^+ e^-) \frac{dM^2}{\pi M^4}, \quad (12)$$

with

$$M \Gamma(\gamma^* \rightarrow e^+ e^-) = \frac{\alpha}{3} (M^2 + 2m_e^2) \sqrt{1 - \frac{4m_e^2}{M^2}} \quad (13)$$

being the decay width of a virtual photon into the dilepton pair with invariant mass M . The last three equations being combined give the $\Delta(1232) \rightarrow Ne^+e^-$ decay rate.

The available experimental data on electro- and photoproduction experiments with $\Delta(1232)$ are fitted in Ref.⁴⁴ using the eVMD framework to give

$$G_M = (2.461 - 0.485M^2 - 0.004M^4)G, \quad (14)$$

$$G_E = (0.062 - 0.010M^2 + 0.004M^4)G, \quad (15)$$

$$G_C = (0.518 - 0.087M^2)G \quad (16)$$

where M^2 is in GeV^2 and

$$G = \prod_{i=1}^4 \frac{m_i^2}{m_i^2 - im_i\Gamma_i(M) - M^2}. \quad (17)$$

The masses m_i of the ρ -meson family members are the following: 0.769, 1.250, 1.450, and 1.720 GeV. The ρ -meson decay rate $\Gamma_1(M)$ is proportional to two-pion phase space and normalized to the vacuum width, whereas $\Gamma_i(M)$ for $i \geq 2$ are set equal to zero, since $M \leq 1$ GeV at our conditions. The quality of the fit can be verified with Fig. 20 of Ref.⁴⁴ Equations (14) - (17) are in agreement with the quark counting rules, the condition $G_M/G_E \rightarrow -1$ at $M^2 \rightarrow -\infty$ is a consequence of the quark counting rules.

7. Microscopic eVMD model

Radially excited ρ - and ω -mesons are introduced^{44,45} to ensure the correct asymptotic behavior of the $RN\gamma$ transition form factors in line with the quark counting rules.⁴⁶ We refer this model as the extended vector meson dominance (eVMD) model. From the experimental side, the excited vector mesons are needed to match photon $M^2 = 0$ and vector meson $M^2 \sim 0.5 \text{ GeV}^2$ experimental branchings of nucleon resonances within a unified scheme.

- The eVMD model provides a unified description of the photo- and electro-production data and of the vector meson and dilepton decays of nucleon resonances and accounts for quark counting rules.

We take constraints on the transition form factors from the quark counting rules into account explicitly. The remaining parameters are fixed by fitting the available photo- and electro-production data and using results of the πN multichannel partial-wave analysis. When data are not available, we used predictions of the additive quark models.

Radially excited ρ - and ω -mesons as a consequence of the quark counting rules interfere with the ground-state mesons *destructively* below the ρ -meson peak and reduce dilepton spectra from decays of nucleon resonances in the vacuum, accordingly.

8. How to keep photon massless with $\rho^0 - \omega - \gamma$ mixing?

VMD model and its modifications introduce mixing of photon with vector mesons ρ^0 , ω , ϕ , etc. Such a mixing can, in principle, generate finite photon mass and destroy gauge invariance. This problem has been solved for VMD model by Kroll, Lee and Zumino⁴⁷ by constructing an effective Lagrangian for photons and vector mesons, which reproduces VMD predictions at a tree level. We describe a distinct consistency proof.

We start from an effective Lagrangian involving pions interacting with photons. An example of such a Lagrangian is e.g. the non-linear sigma model. The vector mesons appear as resonances in two-pion scattering channel (ρ -mesons) and three-meson scattering channel (ω -mesons).

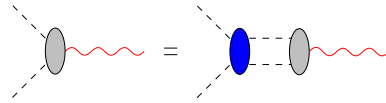


Fig. 6. Diagram representation of the FSI of pions (dashed lines) contributing to form factor in the ρ -meson channel. The wavy lines are photon lines.

Let us consider an absorption of a photon in an isovector channel shown on Fig. 6. Applying two-body unitarity and taking into account analyticity (see e.g.,⁴⁸ Chap. 18), we replace the pointlike vertex e by $eP_l(t)/D_J(t)$ where $t = q^2$ is the photon momentum squared, $P_l(t)$ is a polynomial of the degree l , and $D_J(t)$ is the Jost function defined in terms of the p -wave isovector two-pion scattering phase shift $\delta(t)$:

$$D_J(t) = \exp\left(-\frac{t}{\pi} \int_{t_0}^{\infty} \frac{\delta(t') dt'}{t'(t-t')}\right) \quad (18)$$

where t_0 is the two-pion threshold.

In the no-width approximation, the phase shift accounting for the existence of n resonances is given by

$$\delta(t) = \sum_{i=1}^n \pi \theta(t - m_i^2) \quad (19)$$

where m_i is the mass of the i -th radial excitation of the ρ^0 -meson. Substituting this expression into Eq.(18), we obtain

$$F(t) = P_l(t) \prod_{i=1}^n \frac{m_i^2}{t - m_i^2} \quad (20)$$

(cf. Eqs.(14) - (17)). The requirement $F(t) \rightarrow 0$ at $t \rightarrow \infty$ gives $l < n$.

Analytical functions are fixed by their singularities. The representation (20) can be rewritten in the additive form

$$F(t) = \sum_{i=1}^n c^i \frac{m_i^2}{m_i^2 - t} \quad (21)$$

where c^i are some coefficients. The normalization condition $F(0) = 1$ and quark counting rules impose constraints (sum rules) for c^i .

The effective pion Lagrangian is well defined, since pions are stable particles which exist as asymptotic states. In the approach presented above, the problem of gauge invariance does not appear, since gauge invariance of the effective Lagrangian ensures transverse polarization tensor of photons and the vanishing photon mass. The vector mesons are resonances accounted for by the the final-state interactions (FSI).

9. In-medium properties of vector mesons: What can we learn from observations?

The gap between observables measured in heavy-ion collisions and theoretical models of the in-medium hadrons is filled by transport models which account for complicated dynamics of heavy-ion collisions and provide a link between theory and experiment. We comment results concerning physical properties of in-medium vector mesons that can be derived from experimental data with use of transport models.

9.1. A constraint to ω -meson collision width from DLS and HADES data

In-medium broadening of vector mesons gives an increase of the nucleon resonance decay widths $R \rightarrow NV$ and a decrease of the dilepton branchings $V \rightarrow e^+e^-$ due to enhanced total vector meson widths.

The differential branching $dB(\mu, M)^{R \rightarrow NV}$ of resonance R with an off-shell mass μ increases with the V meson width due to subthreshold character of the vector meson production in light nucleon resonances. The dilepton

branching of the nucleon resonances

$$dB(\mu)^{R \rightarrow Ne^+e^-} \sim dB(\mu)^{R \rightarrow NV} \frac{\Gamma_{V \rightarrow e^+e^-}}{\Gamma_V^{\text{total}}} \quad (22)$$

is, on the other hand, inverse proportional to the *total* vector meson width. This effect is particularly strong for ω , since $\Gamma_{\omega}^{vac} = 8$ MeV only. Fig. 7 shows the collision broadening effect on the dilepton spectra. To get description of the data, we have to assume

$$\Gamma_{\omega}^{\text{total}} \approx \Gamma_{\omega}^{\text{coll}} \geq 50 \text{ MeV} \quad \text{at density } \rho \sim 1.5\rho_0 \quad (23)$$

where ρ_0 is the saturation density. The similar conclusions holds for HADES data.³⁴

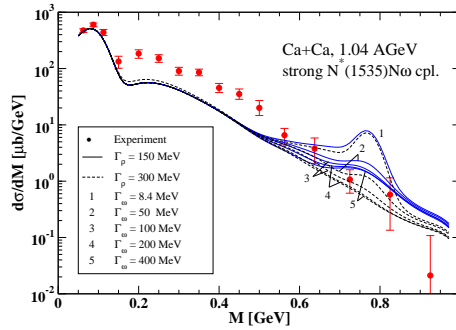


Fig. 7. Dilepton spectra in $Ca + Ca$ collisions for different values of the in-medium ρ and ω widths. The solid curves correspond calculations where the ρ width is kept at its vacuum value of 150 MeV (no collision broadening). The dashed curves correspond to a total ρ width of 300 MeV. In both cases the ω width is varied between $\Gamma_{\omega}^{\text{tot}} = 8.4 \div 400$ MeV. $\Gamma_{\omega}^{\text{tot}} \geq 50$ MeV holds as a conservative constraint (from⁴²).

9.2. Evidence for decoherence in transition form factors of nucleon resonances from DLS and HADES data

Fig. 7 shows an obvious deficit of dileptons below the ρ -meson peak. This phenomenon has been called "DLS puzzle", since transport models were not able to reproduce it. The eVMD suggests a medium-induced decoherence of vector mesons entering transition form factors of nucleon resonances and gives an enhancement of dilepton yield.⁴² It does not remove disagreement with the DLS data completely, however, the recent HADES data³⁴ shown on Fig. 8 are reproduced at $M \leq m_{\rho}$ perfectly.^{34,49} A more detailed theoretical study of the decoherence effect would certainly be welcome.

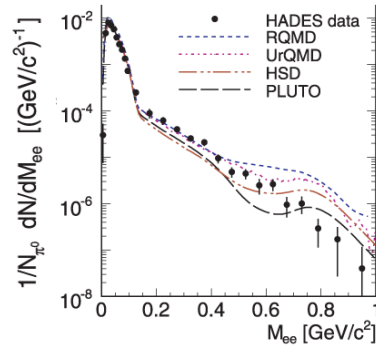


Fig. 8. The experimental dilepton spectrum as compared to predictions of PLUTO³⁴ thermal model, UrQMD,⁴⁰ RQMD,⁴² and HSD³⁶ transport models.

9.3. *No evidence for dropping ρ -meson mass with increasing density from NA60 data*

The NA60 Collaboration presented recently an impressive attempt to extract the ρ -meson spectral function from dilepton spectra at ultrarelativistic heavy-ion collisions.³³ It had not found evidence for a change of the ρ -meson mass. This observation poses obvious difficulties for the Brown-Rho scaling hypothesis.

10. Conclusions

In this lecture, an introduction is made to physics of in-medium behavior of resonances. Transparent methods developed in the atomic spectroscopy in gases can be useful for in-medium hadron spectroscopy. The main topic we focused on is the modifications of spectral functions. Starting from instructive examples in atomic and nuclear physics, we approached the problem of vector mesons description in dense nuclear matter.

Theoretical models are discussed in Sect. 4. The most of them do not go beyond the first order in density. In the non-linear sigma model, density expansion for pions has zero convergence radius.⁵⁰ The higher-order calculations would help to clarify to what extent density expansion for vector mesons is reliable.

This summer (2006 year) two new important experimental works^{33,34} from NA60 and HADES collaborations have been completed and results published. Preliminary conclusions are provided in Sect. 9.

- Collision broadening of ω -meson is constrained from below by ~ 50

MeV at $\rho \sim 1.5\rho_0$ where ρ_0 is the saturation density.

- DLS puzzle had apparently dissolved due to decoherence in in-medium propagation of vector mesons.
- The NA60 data³³ do not provide any evidence for dropping the ρ -meson mass.

Among difficulties in description and interpretation of the HADES data, one has to mention theoretical excess of dileptons above the ρ -peak. The dilepton yield could be suppressed by increasing the ρ and ω collision widths and by taking into account collision broadening of nucleon resonances.

The results of the KEK Collaboration³² show an enhancement below the ρ -peak, which is not understood.

Results of the dilepton production in heavy-ion collisions attract great attention and will certainly be analyzed in future.

References

1. I. I. Sobelman, *Introduction to the Theory of Atomic Spectra*, (Pergamon Press, Oxford, 1972).
2. L. A. Kondratyuk, M. I. Krivoruchenko, N. Bianchi, E. D. Sanctis and V. Muccifora, Nucl. Phys. A **579**, 453 (1994).
3. P. Bogen, Z. Phys. **149**, 62 (1957).
4. N. Bianchi *et al.*, Phys. Lett. B **309**, 5 (1993).
5. J. D. Walecka, Annals Phys. (N.Y.) **83**, 491 (1974).
6. S. A. Chin, Annals Phys. (N.Y.) **108**, 301 (1977).
7. A. Bhattacharyya, S. K. Ghosh and S. C. Phatak, Phys. Rev. **C60**, 044903 (1999).
8. A. Mishra, J. Reinhardt, H. Stocker and W. Greiner, Phys. Rev. **C66**, 064902 (2002).
9. Y. Nambu and G. Jona-Lasinio, Phys. Rev. **122**, 345 (1961); **124**, 246 (1961).
10. K. Tsushima, T. Maruyama and A. Faessler, Nucl. Phys. A**535**, 497 (1991); T. Maruyama, K. Tsushima and A. Faessler, Nucl. Phys. A**537**, 303 (1992).
11. G. E. Brown, Mannque Rho, Phys. Rept. **398**, 301 (2004).
12. A. I. Bochkarev and M. E. Shaposhnikov, Nucl. Phys. B**268**, 220 (1986).
13. E. G. Drukarev and E. M. Levin, JETP Lett. **48**, 338 (1988).
14. C. Adami and G. E. Brown, Phys. Rept. **234**, 1 (1993); T. Hatsuda, H. Shiomi and H. Kuwabara, Prog. Theor. Phys. **95**, 1009 (1996).
15. T. Hatsuda and S.H. Lee, Phys. Rev. **C46**, R34 (1992); S. Leupold, Phys. Rev. **C64**, 015202 (2001).
16. F. Klingl, N. Kaiser, W. Weise, Nucl. Phys. A**624**, 527 (1997).
17. E. G. Drukarev *et al.*, Phys. Rev. **C69**, 065210 (2004).
18. G. Chanfray, Magda Ericson, P. A. M. Guichon, Phys. Rev. **C68**, 035209 (2003).
19. L. A. Kondratyuk *et al.*, Phys. Rev. **C58** (1998) 1078.
20. A. T. Martell, P. J. Ellis, Phys. Rev. **C69**, 065206 (2004).

21. G. E. Brown and M. Rho, Phys. Rev. Lett. **66**, 2720 (1991).
22. A. Gomez Nicola *et al.*, AIP Conf. Proc. **660**, 156 (2003).
23. B. V. Martemyanov, Amand Faessler, C. Fuchs, M. I. Krivoruchenko, Phys. Rev. Lett. **93**, 052301 (2004).
24. R. Rapp, G. Chanfray and J. Wambach, Phys. Rev. Lett. **76**, 368 (1996).
25. F. Klingl, S. Kim, S. H. Lee, P. Morath, W. Weise, Phys. Rev. Lett. **82**, 3396 (1999).
26. S. Digal, P. Petreczky and H. Satz, Phys. Lett. **B514**, 57 (2001).
27. A. Mishra *et al.*, Phys. Rev. **C69**, 015202 (2004).
28. M. C. Abreu *et al.*, Phys. Lett. **423**, 207 (1998).
29. G. Agakichiev *et al.*, Phys. Rev. Lett. **75**, 1272 (1995);
A. Drees, Nucl. Phys. **A610**, 536c (1996).
30. M. Maseara, Nucl. Phys. **A590**, 93c (1995).
31. R. J. Porter *et al.*, Phys. Rev. Lett. **79**, 1229 (1997);
W. K. Wilson *et al.*, Phys. Rev. **C57**, 1865 (1998).
32. K. Ozawa *et al.*, Phys. Rev. Lett. **86**, 5019 (2001).
33. M. Floris *et al.* [NA60 Collaboration], arXiv:nucl-ex/0606023.
34. The HADES Collaboration, arXiv:nucl-ex/0608031.
35. R. Rapp and J. Wambach, Adv. Nucl. Phys. **25**, 1 (2000).
36. W. Cassing and E. L. Bratkovskaya, Phys. Reports **308**, 65 (1999).
37. R. Schneider and W. Weise, Eur. Phys. J. **A9**, 357 (2000).
38. E. L. Bratkovskaya, Phys. Lett. **B529**, 26 (2002).
39. A. Faessler, C. Fuchs, M. I. Krivoruchenko, Phys. Rev. **C61**, 035206 (2000).
40. C. Ernst, S. A. Bass, M. Belkacem, H. Stocker, W. Greiner, Phys. Rev. **C58**, 447 (1998).
41. E. L. Bratkovskaya, W. Cassing, U. Mosel, Nucl. Phys. **A686**, 568 (2001).
42. K. Shekhter, C. Fuchs, Amand Faessler, M. Krivoruchenko, B. Martemyanov, Phys. Rev. **C68**, 014904 (2003).
43. M. I. Krivoruchenko and Amand Faessler, Phys. Rev. **D65**, 017502 (2002).
44. M. I. Krivoruchenko, B. V. Martemyanov, Amand Faessler, and C. Fuchs, Ann. Phys. (N.Y.) **296**, 299 (2002).
45. Amand Faessler, C. Fuchs, M. I. Krivoruchenko and B. V. Martemyanov, J. Phys. **G29**, 603 (2003).
46. V. A. Matveev, R. M. Muradian and A. N. Tavkhelidze, Lett. Nuovo Cim. **7**, 719 (1973);
S. J. Brodsky and G. R. Farrar, Phys. Rev. Lett. **31**, 1153 (1973);
A. I. Vainstein and V. I. Zakharov, Phys. Lett. **B72**, 368 (1978).
47. N. M. Kroll, T. D. Lee and B. Zumino, Phys. Rev. **D157**, 1376 (1967).
48. J. D. Bjorken and S. D. Drell, *Relativistic Quantum Fields*, (New York, McGraw-Hill, 1965).
49. M. D. Cozma, C. Fuchs, E. Santini, A. Fassler, Phys. Lett. **B640**, 170 (2006).
50. M. I. Krivoruchenko, C. Fuchs, B. V. Martemyanov, A. Faessler, arXiv:hep-ph/0505083.